

International Conference on Space Optics—ICSO 2020

Virtual Conference

30 March–2 April 2021

Edited by Bruno Cugny, Zoran Sodnik, and Nikos Karafolas



Overview of PLATO's cameras on-ground and in-orbit calibration and characterisation



Overview of PLATO's Cameras on-ground and in-orbit Calibration and Characterisation

Martin Pertenais^a, Juan Cabrera^b, Denis Griessbach^a, Anders Erikson^b, Bart Vandebussche^c,
Reza Samadi^d, Daniel Reese^d, and Heike Rauer^{b,e,f}

^aGerman Aerospace Center (DLR), Institute for Optical Sensor Systems, Rutherfordstr. 2,
12489 Berlin, Germany

^bGerman Aerospace Center (DLR), Institute for Planetary Research, Rutherfordstr. 2, 12489
Berlin, Germany

^cInstitute of Astronomy, KU Leuven, Celestijnenlaan 200D bus 2401, 3001 Leuven, Belgium

^dLESIA, Observatoire de Paris, Universite PSL, CNRS, 5 place Jules Janssen, 92195 Meudon
Cedex, France

^eInstitute of Geological Sciences, Freie Universität Berlin, Malteserstr. 74-100, D-12249 Berlin,
Germany

^fDepartment of Astronomy and Astrophysics, Berlin University of Technology, Hardenbergstr.
36, D-10623 Berlin, Germany

ABSTRACT

The PLANetary Transits and Oscillations of stars mission (PLATO) is the M3 mission in ESA's Cosmic Vision 2015-2025 Programme, see Rauer et al. (2014).¹ The PLATO mission aims at detecting and characterizing extrasolar planetary systems, including terrestrial exoplanets around bright solar-type stars up to the habitable zone. In order to achieve its scientific objectives, PLATO must perform uninterrupted high precision photometric monitoring of large samples of stars during long periods to detect and characterize planetary transits. The PLATO light curves will also contain information on the seismic activity of the stars, which can help to constrain mass, radii and ages of the exoplanet host stars. The scientific payload of PLATO, developed and provided by the PLATO Mission Consortium (PMC) and ESA, is based on a multi-telescope configuration consisting of 24 Normal Cameras (N-CAM) and 2 Fast Cameras (F-CAM), so as to provide simultaneously a large field of view and a large collecting aperture. The optical design is identical for all cameras and consists of a 6-lens dioptric design with a 120 mm entrance pupil and an effective field of view of more than 1000 deg². The calibration and characterization of PLATO's cameras is a real challenge, especially in terms of quantities: there are 26 Flight Models + 3 Flight Spares + 2 Qualification Models and finally 1 Engineering Model to calibrate. In this context, the on-ground calibration and characterization plan of the cameras was optimized, meaning that all the measurements that can be performed in-orbit will not be calibrated on-ground. Our aim is to give an overview of the on-ground activities planned in the coming years to calibrate and characterize PLATO's cameras. In particular, a detailed description of the geometric calibration used for the Fine Guidance System (FGS) and the focusing calibration will be given. A description of the in-flight calibration plan will then be presented to get the full overview of the calibration and characterization of PLATO's cameras. Calibrating so many cameras in space, without any calibration targets/sources on board, only using pointing capabilities of the satellite, stellar targets and advanced data processing is a key aspect for this mission.

Keywords: PLATO, exoplanet, optical calibration, in-orbit calibration, AIT, AIV

Further author information: (Send correspondence to M. Pertenais: e-mail: martin.pertenais@dlr.de)

1. INTRODUCTION TO PLATO PAYLOAD

1.1 Payload Description

The PLATO payload is made of 24 identical “normal” cameras (N-CAM), 2 “fast” cameras (F-CAM), Ancillary Electrical Units providing electrical power and synchronisation signals to all cameras (two N-AEUs and one F-AEU) and a Data Processing System (DPS). The cameras are mounted on an optical bench which belongs to the spacecraft. The electronic units are accommodated separately from the cameras inside the spacecraft service module.

While the camera design is more detailed in the next section, the data processing system is out of scope for this proceeding. It is composed by Data Processing Units (DPUs) that receive images from the front-end electronics of the cameras (1 N-DPU controls 2 normal cameras, and the F-DPUs are fully redundant to increase reliability of the FGS) and process them before transferring the data products to the Instrument Control Unit (ICU) that compress this data and make the final transfer to the Spacecraft that will downlink it to Ground.



Figure 1. Artist impression of the PLATO Spacecraft with the 26 camera visible. The Electronic Units are hidden behind the radiator visible in front below the cameras. Credits: OHB System AG

An important feature of the PLATO payload is that it is not only used for science operations, but also as Fine Guidance System (FGS). The two fast cameras (F-CAMs) indeed acquire images with a high cadence of 2.5s (against 25s for the normal cameras) thanks to frame-transfer CCDs, that are then processed in the F-DPU by a FGS algorithm that closes the loop with the AOCS system of the Spacecraft to allow for fine pointing capabilities.

As detailed in Ref. 2, the 24 N-CAMs are split into 4 groups of 6 on the Spacecraft, each group being tilted by 9.2° away from the S/C Z axis (equal to the F-CAM Boresight). This allows to increase considerably the total field of view of PLATO without impacting too much the noise budget by keeping several cameras pointing to the same stars, see Ref. 3.

1.2 Camera Design

The N-CAMs are working at a nominal cadence of 25s and are monitoring stars fainter than magnitude 8 (photometry on saturated stars down to magnitude 4 will be possible though). The F-CAMs are working at a cadence of 2.5s and mainly observing stars in the magnitude range 4 to 8, on top of providing information for the FGS. Each camera is split into 3 major sub-systems: a Telescope Optical Unit (TOU), a Focal Plane Assembly (FPA) and a Front End Electronic unit (FEE).

The TOU includes a total of 6 lenses that allows to create an image of a very large field of view of more than 18° radius, see Refs. 4, 5 for more details. A baffle is attached to the entrance protective window of the TOU to limit the straylight coming from other parts of the S/C or other cameras, and from celestial objects like the Moon or the Earth. The baffle also acts as the main thermal radiator of the camera. The TOU is attached with 3 bipods to the FPA.

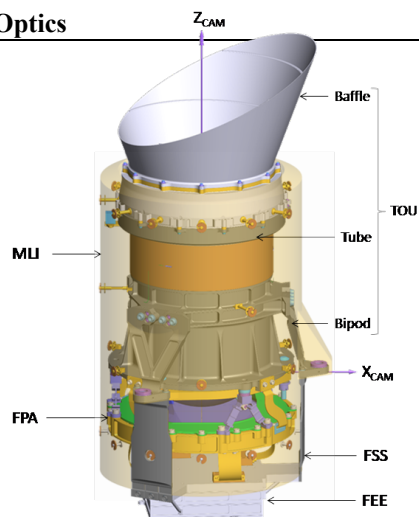


Figure 2. Sketch of a PLATO N-CAM showing the different sub-systems.

The FPA offers a stable structure to support the 4 CCDs that are needed to map the very large field of view of the PLATO cameras. A conductive thermal link is in place between the FPA and the TOU to allow for thermal dissipation of the CCD heat through the Baffle. See Refs. 6 and 7 for more details on the FPA design.

Finally, the FEE unit is mechanically attached to the TOU (for the N-CAM only) and linked to the FPA via the CCD flexis cables. This unit allows reading of the CCD and acquiring of images in the given cadence.

1.3 Focusing Capability

As explained in Ref. 2, the PLATO cameras have the capability to perform optical re-focusing in-orbit using the Thermal Control System (TCS) attached to each camera. The temperature of the camera is indeed actively controlled by the TCS and 3 heaters placed around the pupil position on the conductive tube of the TOU. While the camera as a whole has been designed to be thermally stable (the FPA position compared to the optics of the TOU is stable with temperature), the focus position given by the optics of the TOU has a linear relationship of around 11 $\mu\text{m}/\text{K}$, with the temperature of the camera.

This means that by tuning the controlled temperature of the camera, we can actively refocus the camera. The full range available is from -90°C to -70°C , corresponding to total focus range of $\pm 100 \mu\text{m}$ around the nominal position. This refocusing is needed as the camera is integrated (integration of the FPA to the TOU, see Refs 8 and 9) at ambient condition, while we operate the CAM nominally at -80°C . This range is meant to cover the complete integration error that can occur, as explained in Ref. 2.

1.4 Key parameters to test

Without going into the details of the required calibration and characterization at each sub-system level, the goal of this paper is to describe the key parameters of the cameras that have to be calibrated or characterised at system level.

On the detection chain part, all performance parameters of the CCDs and the FEE are obviously of great interest and have a direct impact on PLATO scientific performance. This includes the quantum efficiency of the CCDs, the Pixel Response Non-Uniformity (PRNU), the linearity curve of the CCD response, the gain, bias, dark, and readout noises of the detection chain.

From the optical point of view, important parameters for the PLATO cameras are mostly the transmission of the optics (as function of field of view position, wavelength and time), and the Point Spread Function (PSF) of the TOU that will drive the size of the image of a star on the detector.

Finally, the combination of the TOU and detection chain, gives us following important parameters at camera level that have to be characterized or calibrated, either on-ground before the launch or directly in-orbit:

- **System PSF:** convolution of the optical PSF, the CCD effect and the focus position
- **Image Geometry:** geometrical model linking the star coordinate in the sky to a pixel coordinate on the CCD
- **Best Focus Position:** calibration of the CAM performance (PSF Size) as a function of the operational temperature of the camera
- **Radiometric performances:** dynamic range, vignetting, ghosts, background level

2. ON-GROUND CALIBRATION AND CHARACTERISATION

Considering the large number of cameras that have to be tested on-ground (26 FMs + 3 Flight Spares + 2 Qualification Models + 1 Engineering Model), the test campaign has to be limited to the important aspects and will be split into 3 parallel Test Houses (IAS in France, SRON in the Netherlands and INTA in Spain).

2.1 Detection chain

For the detection chain of the cameras, most of the characterization and calibration steps are performed at sub-system level as the TOU is not needed to perform them. It is actually easier to perform these tests without the full optics in front of the detectors. For example, all parameters related purely to the CCD, such as quantum efficiency, gain, linearity curve, and PRNU, will be already characterized by the CCD manufacturer Teledyne e2v and FEE providers (MSSL and DLR) before and after coupling with the FPA.

The tests at camera level on the detection chain are therefore limited to the remaining performance parameters that can be monitored with the CAM fully integrated, namely dark measurements and cosmetic defects. The main goals are to verify that the results are consistent with the expectations (delivery from manufacturer and characterization during the analog chain campaign) and to create a set of reference files for the cosmetic defects that will be later considered during in-flight configuration.

For each CCD, a pixel map will be created and updated during the CCD life with the whole cosmetic defects detected, being hot pixels, dead pixels, dead columns, or traps. We will make use of reverse clocking to measure the bias, a functionality which is not operated in-flight. Dark current will be measured at camera level at the operating temperature as a sanity check of the expected CCD performance.

2.2 Best Focus Temperature Determination

For every individual camera, the temperature has to be determined at which the image is best in focus. The best focus temperature is a calibrated parameter needed to reach the best camera performance. In this case, the figure of merit defining the camera best performance is the photometry noise level calculated at system level across the field of view. There is a balance between the PSF extension, the jitter noise, the readout noise, and the impact of stellar contaminants that results in a compromise that can be calculated at system level. Even though the measurement on camera level on-ground before the launch may not be fully representative for the thermal situation on the optical bench and in space, the value is highly useful to reduce the temperature range of other calibrations. On top of that, if the evolution of the PSF with temperature is known, some systematic errors can be partially corrected during the on-ground processing.

To achieve the calibration of these two characteristics (temperature of best focus, and full relation between temperature and focus), the measurement of the transfer function between the size of the PSF and the temperature has to be characterized over the field of view.

The evolution of the PSF size will be measured at 5 TRP1 temperature levels: -90°C , -85°C , -80°C , -75°C , and -70°C . For each of these temperature set-points, the PSF size (the metric used is the ensquared energy in 2x2 pixels) will be measured at 40 positions across the field of view, by rotating the camera in the TV chamber around its entrance pupil until the collimator point source is at the correct position in the field of view. At

each FoV position, multiple integrations are done at different offset positions forming a small raster. Simulations show that 25 sub-positions are needed to recover the maximized ensquared energy. The idea is to compute for each of these 25 positions (that can be raster of a given fraction of pixel, or simply random positions) the figure of merit (in this case the ensquared energy fraction between the brightest 2x2 pixels area and the normalization square e.g. 7x7 pixels) and only save the maximum of these 25 values.

At the end of the FoV scan for a given temperature, the 40 saved values of ensquared energy are averaged (if required using a weighting function) to finally get the averaged ensquared energy for this particular temperature set-point. With the very wide field of view in PLATO, we are indeed not interested in having excellent performance at a given position of field of view if this means having degraded performance somewhere else. We are seeking for homogeneous performance across the whole FoV and we therefore consider the overall distribution of performance (combination of average and standard deviation) over the FoV as our merit function. After all measurements are done, the merit figures (5 points) are plotted against temperature and a fit is made to this curve. The temperature corresponding to the fitted maximum is then established as the optimal focus temperature for this camera.

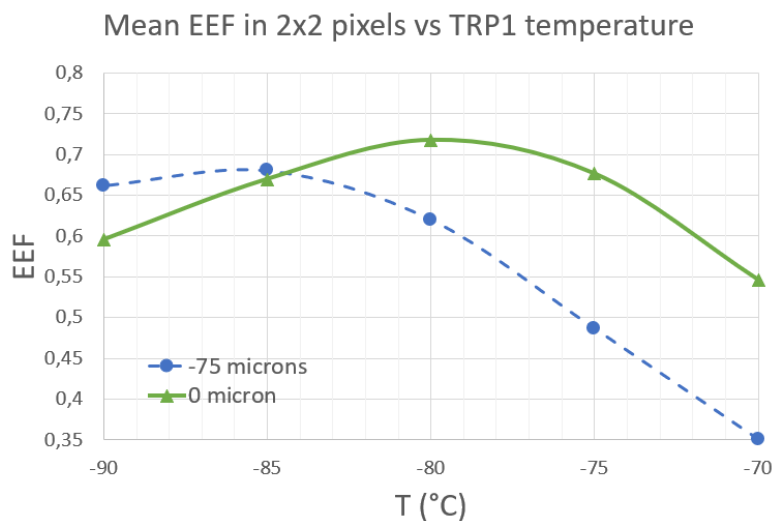


Figure 3. Simulated data plot showing two examples of defocused camera (blue dashed: mechanical defocus of 75 μm , green solid: no mechanical defocus). It represents the averaged (across the FoV) Ensquared Energy Fraction in 2x2 pixels, versus the CAM TRP1 temperature.

Figure 3 shows two examples of such curves that were simulated. The first curve in solid green shows the results of the mean Ensquared Energy over the whole FoV of a N-CAM for the 5 TRP1 temperatures of interest, and considering a "perfect" camera, with its FPA bolted exactly at the best image position of the TOU. In this case, no re-focusing would be needed in theory as the FPA is already mechanically placed at the right position (ambient position leading to the anticipated correct position in cold conditions). This can be recovered with this plot as we clearly see that the maximum of the solid green line, showing the optimal performance of the CAM, coincides well with the nominal operation temperature of -80°C . This virtual CAM would therefore have to be operated at -80°C at TRP1.

The second example in dashed blue, shows a situation where the FPA has been bolted 75 μm away from the TOU best image plane position (again being the ambient position corresponding to the anticipated position at cold). In this case, we observe that the maximum of the curve is around -87°C . This not only confirms the transfer function of around $11 \mu\text{m}/^{\circ}\text{C}$, but also validates the fact that this CAM can be operated correctly as its best focus temperature lies in the achievable range of -90°C to -70°C .

This test is required to be performed on-ground before launch to fully validate the CAM integration and be sure that its best focus temperature is in the achievable range. All further performance characterisation described below is done at the optimal focus temperature determined.

The full temperature-to-PSF size transfer function will also be fully calibrated to be further used while PLATO is in-orbit for potential optimization of data correction. For the F-CAM, this test is even more important, as it will ensure that the F-CAMs are well enough in focus as soon as we turn-on PLATO during the commissioning phase to allow the FGS algorithm to work and provide the fine pointing performance required.

2.3 Image Geometry

The image geometry describes the relation between a direction in the boresight reference frame (e.g. a star coordinate) and the corresponding CCD reference frame (e.g. a pixel number). This geometrical relation, especially the distortion and the focal length, is expected to slightly change with the temperature of the CAM, meaning that this calibration has to be performed for several temperatures around the nominal one to check the sensitivity.

The following parameters are determined:

- Geometrical distortion (including a radial symmetrical and a tangential components) of the optics
- Position of the optical axis with respect to the sensitive area of each CCD.
- Rotation of the sensitive area of each CCD with respect to the camera boresight reference frame, given by the visual reference (only 3 parameters, as a master CCD is defined as reference)
- The effective plate scale of nominally 15 arcsec per pixel (on-axis), defined by the pixel size and the focal length

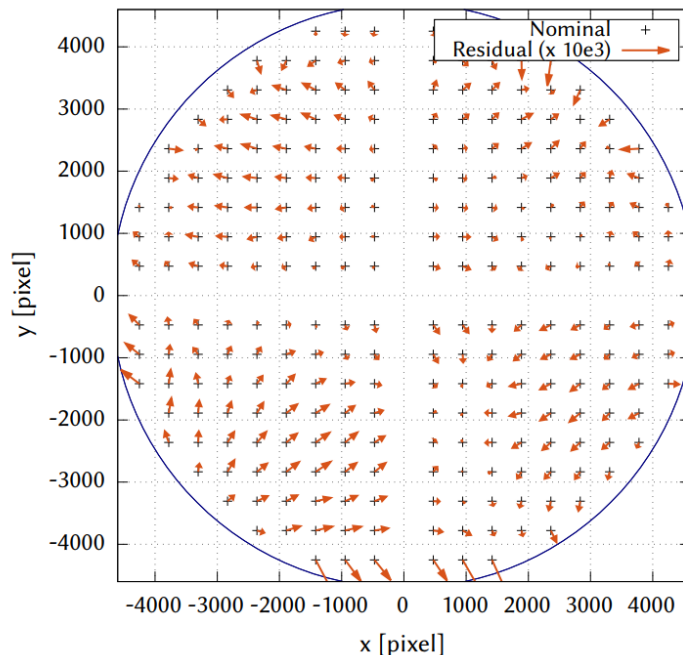


Figure 4. Example of residual error of the camera geometrical model. See Ref. 10 for more details.

This geometrical camera model is needed before launch to anticipate the positions of the stars on the CCDs at the beginning of operations in-orbit, during the commissioning phase. This will then be used for field identification and imagettes (small extracts of a full-frame image) placement for both science targets and calibration targets, e.g. scientific calibration, background in less crowded sky area. On the other side, this geometrical camera model plays a key role for the F-CAMs in the FGS algorithm. It has therefore to be calibrated on-ground before launch to ensure the FGS can initialize when the PLATO payload will be turn on for commissioning.

2.4 Other Optical Characteristics

While the ghost characterization, the best focus determination and the image geometry tests are the main calibration and characterization tests at camera level (i.e. not considering the tests at TOU or detection chain level) required on-ground, several other tests will be performed to fully verify the camera performance. The list below give a non-exhaustive overview of the performance tests that will be performed on-ground and not described in this paper:

- Verification of the PSF Size at the best focus temperature
- Verification of out of field straylight level, as well as expected ghost positions and relative intensities
- Camera Dynamic Range capabilities
- Verification of the long-term (14h) stability of the camera noise and detection gain/SNR

3. IN-ORBIT CALIBRATION AND CHARACTERISATION

3.1 Full-Frame Images

The first step in-orbit, before starting dedicated calibration activities, is to acquire at least a full-frame image for each camera and download it to ground for several processing steps.

This is indeed needed to finalize the field identification from which the reference stars and background window positions can be derived. The background model used during operation can be fine-tuned, as well as the parameters used in the model for CTI correction. On top of this, the CCD pixel maps mentioned earlier will also be updated to track cosmetic defects over all 104 CCDs of the PLATO payload.

It has to be noted that these images will be acquired using the best focus temperatures determined on-ground for each camera. As we expect these to be slightly different in orbit, these initial full-frame images might not show optimal performances.

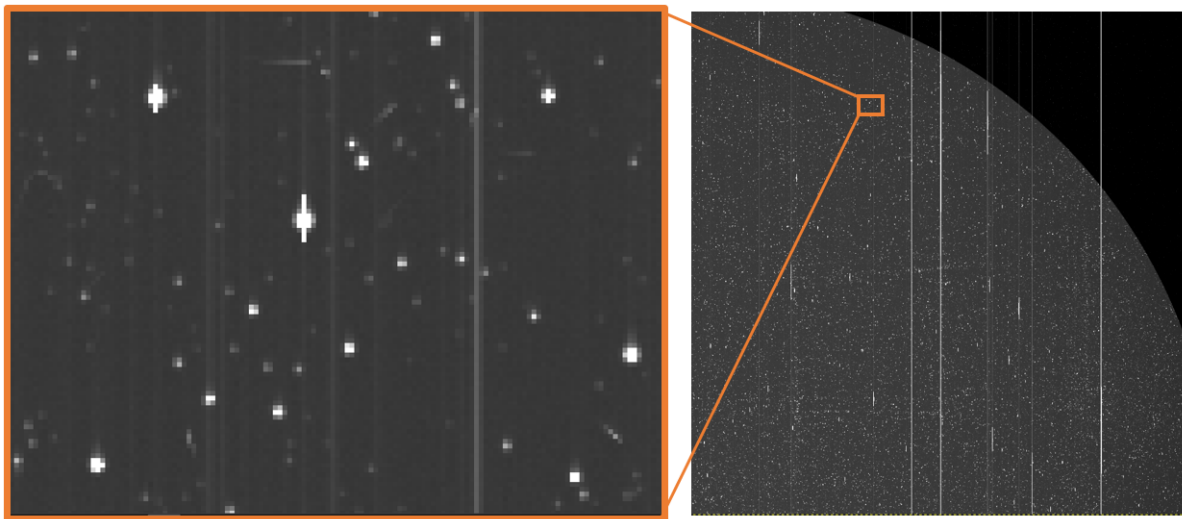


Figure 5. Example of a simulated full-frame image of one CCD (a fourth of a CAM) on the right hand-side, using PLATOSim.^{11,12} The left hand-side shows a zoom insight of a CCD area showing in more details the PSFs of the stars, some saturation effects and CCD effects that are being simulated.

3.2 Best Focus

3.2.1 General focus calibration as a function of temperature

As explained in Section 2.2, each camera will be individually calibrated on-ground before the launch to determine its own best focus temperature. This ensures that each camera will be operated at the temperature maximizing its optical performance. However, because of launch effects as well as environment differences (e.g. gravity release, thermal gradient), this best focus temperature can slightly shift between the on-ground calibration and the in-orbit operations. To overcome this, the best focus determination test will be repeated in-orbit will all cameras using the nominal temperature computed on-ground as starting point.

Performing this calibration directly in-orbit has many advantages compared to the on-ground. Indeed, in terms of schedule, using the chance of having several thousands of stars spread across the FoV that can be observed simultaneously will allow us to reduce drastically the time required to perform this test. This adds to the fact that considering a negligible thermal cross-talk between neighboring cameras, we can perform this calibration of all the 24 normal cameras simultaneously. Finally, the test environment will be obviously more representative as on-ground as it will be exactly the same as during science operations. Thanks to these points, we expect the in-orbit test to be much more accurate than the one on-ground that is therefore mostly used to verify the camera integration success and provide a working starting point for the payload commissioning in-orbit.

To perform this test, time series of imagerie data of a sample of stars will be acquired for each camera and sent to ground for several (current baseline is 11 steps) temperature set-points at TRP1 within the full operating range of $[-90^{\circ}\text{C} ; -70^{\circ}\text{C}]$. A couple of extra temperature points might be added at and around the best focus temperature determined on-ground to increase the final accuracy.

The final output of this in-orbit test is mainly the newly defined 26 nominal operation temperatures of the cameras (one per camera).

3.2.2 Special Cases for the Fast Cameras

As this test determines the nominal operational temperature for each camera (including the F-CAMs), it has to be performed before any other activities. However, to ensure sufficient accuracy, the nominal pointing performances are required to be achieved during this test.

For this, it is mandatory for the fast cameras to deliver images to the FGS algorithm allowing it to converge and stabilize the PLATO pointing as required. It has been showed that even if the full performances are not achieved, the FGS algorithm provides compliant performances even with strongly defocused images, see 10.

To ensure anyway the best focus calibration possible, the following conservative approach has been defined for the full payload calibration:

- Focus calibration of both F-CAMs at the same time (with slightly degraded FGS performance close to the requirements) using the on-ground calibrated best focus temperatures.
- Focus calibration of F-CAM 1 while using F-CAM 2 in its best focus temperature found in the first step.
- Focus calibration of F-CAM 2 and all N-CAMs while using F-CAM 1 in its best focus temperature found in the second step.

3.3 Image Geometry and full-throughput of the Cameras

As for the best focus determination, the image geometry calibration test is an in-orbit repetition of the on-ground calibration explained in Section 2.3. The aim of this calibration is to achieve a distortion map on the whole field of view within a sufficient accuracy and its evolution with temperature for each camera. This is not only needed for the F-CAM for the FGS algorithm, but also for all N-CAMs in order to correctly place window around the star of scientific interests.

Similarly to the image geometry, the absolute and relative throughput of each camera will be characterized in-orbit. While this characterization is very challenging on-ground, due to test setup instabilities, we will use some

reference stars to derive the full throughput of each camera. Indeed, by measuring the flux of several thousands of non-saturated well-known bright stars, the camera throughput as a function of the field of view position can be derived. This full throughput is a combination of the real entrance pupil size of the camera, its real spectral transmission (including contamination), the natural and mechanical vignetting off-axis, the quantum efficiency and detectors performance.

For both of these tests, imagette time series of a chosen sample of stars will be acquired and sent on-ground for analysis for several temperature steps around the best focus temperature of each camera. This will allow to calibrate the models on-ground as a function of the temperature.

3.4 Point-Spread Function (PSF)

As part of the scientific photometric calibration, high-resolution PSFs are required in the pipeline to maximize the photometric extraction accuracy, as described in Ref. 13. Obtaining high-resolution PSFs of the PLATO camera is not a straight-forward task as the pixels used in the camera's FPA are of similar size as the PSFs themselves. We expect the optical PSFs to be spread over approximatively 4x4 pixels.

Building a super-resolved PSF from pixel-resolved images is possible through the exploitation of subpixel motion of the satellite. In order to reconstruct a high-resolution image of the PSF, one needs to solve an inverse problem, using a set of multiple low-resolution images acquired with different sub-pixel displacements of the camera.

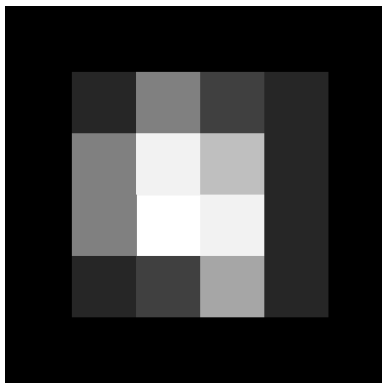


Figure 6. Example of a sampled PSF with PLATO pixels, showing the need for a high-resolution PSF determination concept.

3.4.1 Description of the Micro-scanning Technique

Samadi et al. (2019)¹⁴ describes in detail the micro-scanning technique envisaged for PLATO, in order to re-construct these high-resolutions PSFs. The global principles are simply recalled here.

By pointing the satellite, and as a consequence all 26 cameras, to slightly different positions by following, for instance, the Archimedean spiral pattern shown in Fig. 7, we will acquire a number (baseline is 430) of low-resolution PSFs for different PSF centroid sub-pixel positions.

While the actual pattern is not driving the algorithm (the spiral pattern was chosen for its relatively simple and smooth geometry, as well as the benefit of being mostly independent of orientation making it more robust to any rotations which intervene in the CCD frame of reference), the knowledge of the pointing direction for each acquisition is the deciding factor. This means, that it is very important to have an accurate knowledge of the pointing direction (each red dot position in Fig. 7) associated with each frame acquired. For this purpose, there are very strict requirements on the spacecraft platform and FGS algorithm to achieve better than 300 mas half cone angle attitude Knowledge Drift Error (KDE) over 5 seconds, at a 95% confidence level, for the directional direction of each CAM boresight, and 600 mas for the rotational direction around each CAM boresight. To achieve this performance, on-ground post-processing will be applied based on the fine guidance system and the gyro measurements. The total duration of this operation is expected to be less than 3 hours

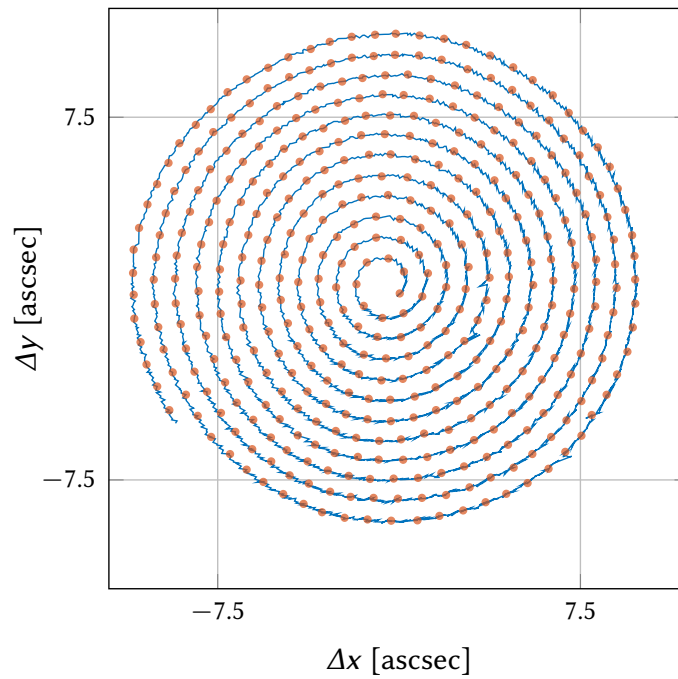


Figure 7. Spiral pattern that will be followed by the spacecraft. Note that a PLATO pixel on-axis corresponds to 15 arcsec.

3.4.2 PSF Inversion and Modelling

Using these 430 low resolution PSFs, the high-resolution PSF will be reconstructed on ground using custom inversion techniques, with a sub-pixel resolution equivalent to 1/20th of a pixel. The PSF is decomposed using cubic B-splines with 20 coefficients per pixel in both directions.

Several inversion techniques have been simulated with PLATO PSFs in Ref. 14, with better results found using a regularised least-square approach, based on a 2D Laplacian multiplied by a weight function. An example of a high-resolution PSF, retrieved using the micro-scanning technique based on a PLATO simulated PSF, is shown in Fig. 8.

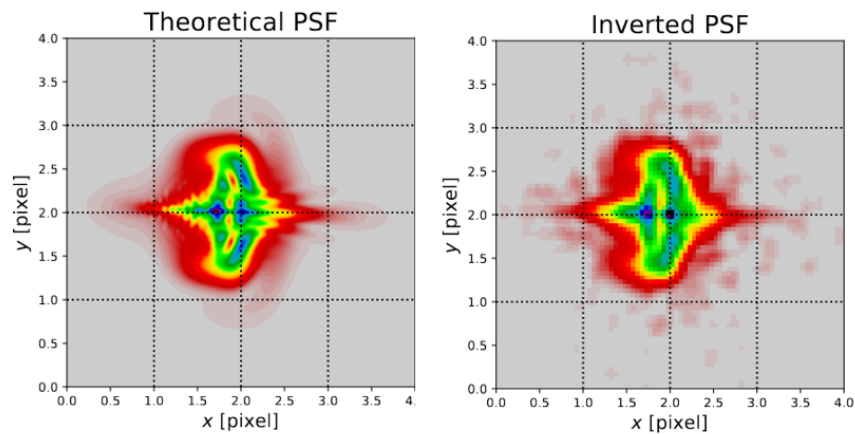


Figure 8. An example of the inversion technique applied to a simulated PLATO optical PSF after micro-scanning measurements. Credits: Samadi et al. (2019)¹⁴

Fig. 8 shows an example of a theoretical PSF on the left hand side that was used as input to test and verify the micro-scanning and inversion technique algorithms. Using a set of 430 low-resolution equivalent PSFs, the inversion algorithm was able to reconstruct the high-resolution PSF on the right hand side. A few artefacts are of course present but the overall performance of the technique is excellent. It has to be noted that this was done on a pure optical PSF including therefore very high frequency components that will actually be smoothed out by the CCD charge diffusion in reality. The result with actual data is therefore expected to be even better.

4. CONCLUSION AND OUTLOOK

Driven by the large number of flight models to be characterized, validated, and calibrated, the characterisation and calibration plan of PLATO's camera has been tailored to the minimum needed and to the tests that cannot be performed in-orbit or required before commissioning. This means that (taking the pure verification tests out of the discussion here) the on-ground calibration campaign will mainly focus on 2 tests: the camera geometrical model translating sky coordinates into pixel coordinates on the FPA, and the best focus temperature determination to determine the individual optimal nominal temperature for each camera.

Using the outcome of these tests as starting point, they will be repeated in-orbit during the payload commissioning phase to assess the changes that occurred during launch and because of environment changes (between the test setup on-ground and the actual operational environment in orbit). These tests are critical especially for the nominal functioning of the Fine-Guidance System using the F-CAMs images as input to achieve the challenging pointing requirements needed for the science cases of PLATO.¹ Finally, by following a well-defined pattern with the PLATO satellite and acquiring hundreds of low-resolution PSFs for different sub-pixel position, the high-resolution PSFs will be retrieved on-ground with inversion techniques.¹⁴ These are needed for the processing pipelines of the PLATO science data products to optimize the photometric extraction.¹³

This calibration and characterisation plan being now well consolidated, the first model of the camera (namely the Engineering Model) will be tested following these procedures during the year 2021 and hopefully bring valuable lessons learned to optimize the plan even more for the FMs and eventually the commissioning of PLATO in-orbit.

ACKNOWLEDGMENTS

This work has benefited from financial support by DLR in the framework of its contribution to the PLATO Mission, as well as CNES and the Belgian Federal Science Policy Office (BELSPO) in the framework of the PRODEX Programme of ESA. This work presents results from the European Space Agency (ESA) space mission PLATO. PLATO data are being processed by the PLATO Mission Consortium (PMC). Funding for the PMC is provided by national institutions, in particular the institutions participating in the PLATO MultiLateral Agreement (MLA). The PLATO mission website is <https://www.cosmos.esa.int/plato> and Mission Consortium website is <https://platomission.com/>.

REFERENCES

- [1] Rauer, H., Catala, C., Aerts, C., Appourchaux, T., Benz, W., Brandeker, A., Christensen-Dalsgaard, J., Deleuil, M., Gizon, L., Goupil, M.-J., and et al., "The plato 2.0 mission," *Experimental Astronomy* **38**, 249–330 (Sep 2014).
- [2] Pertenais, M., Cabrera, J., Paproth, C., Boerner, A., Griessbach, D., Mogulsky, V., and Rauer, H., "The unique field-of-view and focusing budgets of PLATO," *Proc. SPIE* **XX**, XX (2021).
- [3] Ragazzoni, R., Magrin, D., Rauer, H., Pagano, I., Nascimbeni, V., Piotto, G., Piazza, D., Levacher, P., Schweitzer, M., Basso, S., Bandy, T., Benz, W., Bergomi, M., Biondi, F., Boerner, A., Borsa, F., Brandeker, A., Brändli, M., Bruno, G., Cabrera, J., Chinellato, S., Roche, T. D., Dima, M., Erikson, A., Farinato, J., Munari, M., Ghigo, M., Greggio, D., Gullieuszik, M., Klebor, M., Marafatto, L., Mogulsky, V., Peter, G., Rieder, M., Sicilia, D., Spiga, D., Viotto, V., Wieser, M., Heras, A. M., Gondoin, P., Bodin, P., and Catala, C., "PLATO: a multiple telescope spacecraft for exo-planets hunting," in [*Space Telescopes and Instrumentation 2016: Optical, Infrared, and Millimeter Wave*], MacEwen, H. A., Fazio, G. G., Lystrup, M., Batalha, N., Siegler, N., and Tong, E. C., eds., **9904**, 731 – 737, International Society for Optics and Photonics, SPIE (2016).

- [4] Magrin, D., Munari, M., Pagano, I., Piazza, D., Ragazzoni, R., Arcidiacono, C., Basso, S., Dima, M., Farinato, J., Gambicorti, L., Gentile, G., Ghigo, M., Pace, E., Piotto, G., Scuderi, S., Viotto, V., Zima, W., and Catala, C., “PLATO: detailed design of the telescope optical units,” in [*Space Telescopes and Instrumentation 2010: Optical, Infrared, and Millimeter Wave*], Jr., J. M. O., Clampin, M. C., and MacEwen, H. A., eds., **7731**, 715 – 722, International Society for Optics and Photonics, SPIE (2010).
- [5] Magrin, D., “Plato telescope optical units: An update on working status,” in [*Space Telescopes and Instrumentation 2020: Optical, Infrared, and Millimeter Wave*], *Society of Photo-Optical Instrumentation Engineers (SPIE) Conference Series* **11443-80** (2020).
- [6] Moreno, J., Vielba, E., Manjón, A., Motos, A., Vázquez, E., Rodríguez, E., Saez, D., Sengl, M., Fernández, J., Campos, G., Muñoz, D., Mas, M., Balado, A., Ramos, G., Cerruti, C., Pajas, M., Catalán, I., Alcacera, M. A., Valverde, A., Pflueger, P., and Vera, I., “PLATO FPA. focal plane assembly of PLATO instrument,” in [*International Conference on Space Optics; ICSO 2018*], *Society of Photo-Optical Instrumentation Engineers (SPIE) Conference Series* **11180**, 111803N (July 2019).
- [7] Ramos, G., Guijarro, A. L. V., Rodrigo, M. T., Sierra, M. A., Gómez, L. J., Borreguero, E., Álvarez, L., Manjón, A., Balado, A., Barrado, D., and Mas, J. M., “Planetary transits and oscillation of stars (PLATO) focal plane assembly (FPA): prototype assembly and integration verification,” in [*UV/Optical/IR Space Telescopes and Instruments: Innovative Technologies and Concepts IX*], Barto, A. A., Breckinridge, J. B., and Stahl, H. P., eds., **11115**, 49 – 59, International Society for Optics and Photonics, SPIE (2019).
- [8] Clermont, L., Jacobs, J., Blain, P., Abreu, M., Vandenbussche, B., Royer, P., Huygen, R., Halain, J. P., and Baeke, A., “Automatized alignment of the focal plane assemblies on the PLATO cameras,” in [*Space Telescopes and Instrumentation 2018: Optical, Infrared, and Millimeter Wave*], Lystrup, M., MacEwen, H. A., Fazio, G. G., Batalha, N., Siegler, N., and Tong, E. C., eds., **10698**, 1902 – 1913, International Society for Optics and Photonics, SPIE (2018).
- [9] Royer, P., L. Clermont, J., M. Pertenais, A. Baeke, Huygen, R., J. De Ridder, Regibo, S., M. Dami, Vandenbussche, B., A. Belen Balado Margeli, J. Farinato, D. Greggio, Y. Levillain, D. Magrin, L. Marafatto, M. Pajas, G. Ramos Zapata, A.L. Valverde Guijarro, and V. Viotto, “On the optical alignment of the PLATO cameras,” in [*Space Telescopes and Instrumentation 2020: Optical, Infrared, and Millimeter Wave*], *Society of Photo-Optical Instrumentation Engineers (SPIE) Conference Series* **11443**, 111443L (Aug. 2020).
- [10] Griessbach, D., Witteck, U., and Paproth, C., “The Fine Guidance System of the PLATO Mission ,” **XX**, SPIE (2021).
- [11] De Ridder, J., “PlatoSim: A simulator for the PLATO Camera,” *Astronomy & Astrophysics in prep.* (2021).
- [12] De Ridder, J., Royer, P., Regibo, S., Huygen, R., Vandenbussche, B., De Meester, W., and Tkachenko, A., “The PlatoSim simulator: A tool for payload performance assessment and science objective verification,” in [*Space Telescopes and Instrumentation 2020: Optical, Infrared, and Millimeter Wave*], *Society of Photo-Optical Instrumentation Engineers (SPIE) Conference Series* **11443**, 111443L (Aug. 2020).
- [13] Marchiori, V., Samadi, R., Fialho, F., Paproth, C., Santerne, A., Pertenais, M., Börner, A., Cabrera, J., Monsky, A., and Kutrowski, N., “In-flight photometry extraction of PLATO targets. Optimal apertures for detecting extrasolar planets,” **627**, A71 (July 2019).
- [14] Samadi, R., Deru, A., Reese, D., Marchiori, V., Grolleau, E., Green, J. J., Pertenais, M., Lebreton, Y., Dehevels, S., Mosser, B., Belkacem, K., Börner, A., and Smith, A. M. S., “The PLATO Solar-like Light-curve Simulator. A tool to generate realistic stellar light-curves with instrumental effects representative of the PLATO mission,” **624**, A117 (Apr. 2019).